Observations of iodine monoxide over three summers at the Indian Antarctic bases, Bharati and Maitri

Anoop S. Mahajan[1*], Mriganka S. Biswas[1,2], Steffen Beirle[3], Thomas Wagner[3], Anja Schönhardt[4], Nuria Benavent[5] and Alfonso Saiz-Lopez[5]

[1]Centre for Climate Change Research, Indian Institute of Tropical Meteorology, Ministry of Earth Sciences, Pune, 411008 India.

[2]Savitribai Phule Pune University, Pune, 411008 India.

[3]Max-Planck-Institut für Chemie (MPI-C), Satellitenfernerkundung, 55128 Mainz, Germany

[4]Institute of Environmental Physics, Department of Physics and Electrical Engineering, University of Bremen, Bremen, 330440 Germany.

[5]Department of Atmospheric Chemistry and Climate, Institute of Physical Chemistry Rocasolano, CSIC, Madrid 28006, Spain

* corresponding author: Anoop S. Mahajan (anoop@tropmet.res.in)

Abstract

Iodine plays a vital role in oxidation chemistry over Antarctica, with past observations showing highly elevated levels of iodine oxide (IO) leading to severe depletion of boundary layer ozone in West Antarctica. Here, we present multi axis differential absorption spectroscopy (MAX-DOAS) based observations of IO over three summers (2015-2017) at the Indian Antarctic bases, Bharati and Maitri. IO was observed during all the campaigns, with mixing ratios below 2 pptv for the three summers, which are lower than the peak levels observed in West Antarctica. This suggests that sources in West Antarctica are different or stronger than sources of iodine compounds in East Antarctica, the nature of which are still uncertain. Vertical profiles estimated using a profile retrieval algorithm showed decreasing gradients, with a peak in the lower boundary layer. The ground-based instrument retrieved vertical column densities (VCDs) were approximately a factor of three-five higher than the VCDs reported using satellite-based instruments, which is most likely related to the sensitivities of the measurement techniques. Airmass back-trajectory analysis failed to highlight a source region, with most of the airmasses coming from coastal or continental regions. This study highlights the variation in iodine chemistry in different regions in Antarctica and the importance of a long-term dataset to validate models estimating the impacts of iodine chemistry.

Keywords: Iodine; Antarctica; halogens; DOAS

1. Introduction

Reactive halogen species (RHS) have been shown to play a critical role in causing ozone depletion events in the polar boundary layer (BL) (Barrie et al., 1988; Bottenheim et al., 1986; Kreher et al., 1997; Oltmans and Komhyr, 1986) and could contribute to new particle formation in this remote environment (Allan et al., 2015; Atkinson et al., 2012; O'Dowd et al., 2004). Observations of RHS have been made in the Antarctic BL for almost two decades. Early observations focused on bromine oxide (BrO), the presence of which was observed in the Antarctic using ground based instruments (Kreher et al., 1997) and via satellites (Hollwedel et al., 2004). The presence of iodine oxide (IO) in the Antarctic atmosphere was also confirmed through integrated column measurements from the ground (Frieß et al., 2001). Later, year-long ground-based observations of RHS made at Halley Bay showed the critical role that bromine and iodine compounds play in regulating the oxidizing capacity, causing ozone depletion and new particle formation in the Antarctic BL (Saiz-Lopez et al., 2007a). These ground-based observations showed that both IO and BrO, are present at elevated concentrations (from 1 pptv to as high as 20 pptv) in certain parts of the Antarctic BL, and show a significant seasonal variation peaking in the spring, with elevated concentrations observed through the summer (Saiz-Lopez et al., 2008). Satellite-based observations of both IO and BrO reported a similar annual cycle, although with large geographical differences (Hollwedel et al., 2004; Richter et al., 2002; Saiz-Lopez et al., 2007b; Schönhardt et al., 2008, 2012; Theys et al., 2011; Wagner et al., 2001). These satellite observations have been validated by ground-based observations, although most of them have hitherto focused around the Weddell Sea (Atkinson et al., 2012; Buys et al., 2013; Frieß et al., 2001, 2010; Saiz-Lopez et al., 2007a, 2008). Previous studies show that similar levels of BrO have been observed between the Arctic and Antarctic while much lower levels of atmospheric iodine have been reported in the

Arctic compared to the Antarctic (Hönninger et al., 2004; Raso et al., 2017; Schönhardt et al., 2008; Tuckermann et al., 1997). The satellite observations also show a difference in the geographical distribution of IO over Antarctica, with the Weddell sea being an iodine hotspot, the reasons for which are still not completely clear (Saiz-Lopez and Blaszczak-boxe, 2016). Ground-based observations have also been made at McMurdo Sound, near the Ross Sea, where lower concentrations of IO were observed (Hay, 2010). Additional observations over the 2011-2012 summer were made at Dumont d'Urville using a cavity enhanced absorption spectroscopy based instrument and showed a maximum of 0.15 pptv of IO (Grilli et al., 2013). However, observations of IO have not been reported in the Indian Ocean sector of the Antarctic peninsula to date (Saiz-Lopez et al., 2012; Saiz-Lopez and von Glasow, 2012).

Ground based observations at Halley Bay and in the Weddell Sea suggest that the main source of iodine compounds is the sea ice region based on observations of iodocarbons and back trajectory analysis (Atkinson et al., 2012; Saiz-Lopez et al., 2007a). Other studies have also measured iodocarbons in Antarctica, although their levels are too low to explain the high levels observed in the Weddell Sea region (Carpenter et al., 2007; Fogelqvist and Tanhua, 1995; Reifenhäuser and Heumann, 1992). The exact process is still not known, although a mechanism for biologically-induced iodine emissions from sea-ice has been suggested based on the idea that micro-algae (Garrison and Buck, 1989) are the primary source of iodine emissions in this environment (Saiz-Lopez et al., 2015a) with halogen compounds then moving up brine channels in the sea ice to finally get released into the atmosphere. There are further questions regarding the propagation of reactive iodine chemistry across the continent because satellite observations show the presence of IO deep within the Antarctic continent, even as far as the South Pole (Saiz-Lopez et al., 2007b; Schönhardt et al., 2008). However, although enhanced, the observed IO column densities are close

to the detection limit of the satellite instrument (~7 x 10^{12} molecules cm^{-2} for a single measurement) and are therefore subject to uncertainties. The study by Frieß et al. (2010) suggested a strong source within the snowpack, which hints at active recycling and re-emission of IO aiding the long transport inland. However, questions remain about why such a source would function only in parts of the continent and why the primary source is different from the Arctic, where much lower peak concentrations are sporadically observed (Mahajan et al., 2010; Saiz-Lopez and Blaszczak-boxe, 2016). To further understand the sources of iodine in the polar environment, understanding the geographical distribution is critical. Satellite observations play a useful role for this, although validation of the satellite observations using ground-based instruments is necessary to ascertain their accuracy to observe IO in the Antarctic troposphere.

Questions also remain about the vertical profiles of iodine compounds within and above the Antarctic boundary layer. Modelling based studies using the one-dimensional Tropospheric Halogen Chemistry MOdel (THAMO) have suggested a strong gradient in IO from the surface to the edge of the boundary layer (Saiz-Lopez et al., 2008). Only once in the past have vertical profiles of IO been measured in Antarctica. These measurements were made at McMurdo Sound in East Antarctica (Hay, 2010). Observations over two "golden days" in 2006 and 2007 show surface concentrations of about 1 pptv, decreasing to ~0.2 pptv at about 200 m, before reaching a second maximum of 0.6 pptv at ~700 m. However, models did not reproduce this measured IO vertical profile shape and there are also large uncertainties associated with the a priori (Hay, 2010). In most models, the assumption is that the source of iodine compounds is from the snowpack, with photochemistry in the atmosphere resulting in a steady decrease with altitude. However, considerable challenges remain in reproducing the surface variation and vertical gradients in addition to the geographical distribution (Fernandez et al., 2019). More recent modelling studies

combined with aircraft observations suggest that the gradient is not very sharp all the latitudes, with a significant free tropospheric and stratospheric contribution to the total column of IO (Koenig et al., 2020; Saiz-Lopez et al., 2015b), although such observations have still not been done in the Antarctic. One of the main reasons for the uncertainties in models is the lack of consistent measurements of vertical gradients across the world, especially in the Polar Regions, to validate these model simulations.

Considering the uncertainties in the satellite observations and questions regarding the sources and vertical and geographical distribution of IO, further observations are necessary. Here we present observations made at two new locations in Antarctica over three summers and compare them with the satellite-based retrievals and past observations.

2. Methodology

Figure 1 shows the location of the two Indian Antarctic stations, Maitri (11.73 °E , 70.77 °S) and Bharati (76.19 °E, 69.41 °S). The other stations where observations of IO have been reported in the past are also marked on the map. Observations of IO and the oxygen dimer (O_4) were made using the Multi-Axis Differential Optical Absorption Spectroscopy technique (MAX-DOAS) over three summers: February-March 2015 as a part of the 34th Indian Scientific Expedition to Antarctica (ISEA-34), November 2015 – February 2016 as a part of ISEA-35 and January-February 2017 as a part of ISEA-36.

Observations at the Maitri station were made over a short span of 9 days (9th March – 17th March 2015) and only during ISEA-34. The research station is in the ice-free rocky area on the Schirmacher Oasis. The MAX-DOAS instrument was installed in a summer-time residential

container, ~150 m north the station, about 120 m above sea level during the ISEA-34. The scanner unit was mounted on top of the container with the clear line of sight to the horizon. The scanner pointed ~60.0° with respect to magnetic north. The spectrometer unit was kept inside the container, which was temperature controlled. The open ocean is 125 km north of Maitri.

Observations at the Bharati station were made for 10 days (9th February-18th February 2015) during ISEA-34, for 63 days (30th November 2015 – 1st February 2016) during ISEA-35 and for 35 days (5th January-11th February 2017) during ISEA-36. The station is located between the Thala Fjord and Quilty Bay, east of the Stornes Peninsula. The MAX-DOAS instrument was installed in a hut on top of a ridge around 200 m south-west of the Bharati station and was approximately 56 m above sea level. The scanner unit was mounted on the wall of the hut and had a clear line of sight to the horizon, pointing -23.2° with respect to the north, overlooking the open ocean. The coastline is within 500 m of the hut, but it becomes ice free from mid-January to late March. Depending on the sea ice conditions, the open ocean is within 8-10 km north from the end of November.

The MAX-DOAS instrument (EnviMes) makes use of scattered sunlight along different elevation angles and by combination of several lines of sight including the zenith. The concentration of an absorber in the boundary layer can be obtained either in a first approximation by a simple geometric approach or by simulating the light path with a radiative transfer model taking into account also multiple scattering effects and the correct treatment of the aerosol loading in the atmosphere (Hönninger et al., 2004; Platt and Stutz, 2008; Wagner et al., 2004). The instrument consists of an indoor unit, housing a spectrometer with a spectral resolution of 0.7 nm (UV: 301.20-463.69), which is connected to an outdoor unit, containing a scanning telescope. Discrete elevation angles (1°, 2°, 3°, 5°, 7°, 10°, 20°, 40°, and 90°) were recorded for a total exposure time of 1 minute each during all the four campaigns. The spectra were recalibrated before analysis using

mercury emission lines recorded at the end of each day. For DOAS retrieval, the QDOAS 3.2 software was used (Fayt and Van Roozendael, 2013). For estimation of the O_4 Differential Slant Column Densities (DSCDs), the cross-sections of O_4 (Thalman and Volkamer, 2013) at 293K; NO_2 (Vandaele et al., 1998) at 220 K and 298 K (220 K orthogonalized to 294 K); O_3 (Bogumil et al., 2003) at 223 K and 243 K (orthogonalized to O_3 at 243 K); HCHO (Meller and Moortgat, 2000) at 298 K; HONO (Stutz et al., 2000) at 296 K were used in the 351-390 nm window. The cross-sections used for IO retrieval in the 417-440 nm spectral window were: IO (Gómez Martín et al., 2005), NO_2 220 K and 298 K (Vandaele et al., 1997), H_2O (Rothman et al., 2013), O_4 (Thalman and Volkamer, 2013) and O_3 (Bogumil et al., 2003). In addition to these cross-sections a ring spectrum (Chance and Spurr, 1997), a second ring spectrum following Wagner et al. (2009), and the 3rd order polynomial were used for both windows. The zenith spectrum from each scan was used as a reference to remove contribution from possible free tropospheric or stratospheric absorption. An example of a DOAS fit for O_4 and IO are given in Figure S1. Surface mixing ratios and the total vertical column densities (VCDs) were retrieved from the MAX-DOAS DSCDs of IO and O_4 by employing the Mainz Profile Algorithm (MAPA) (Beirle et al., 2018). Only observations with solar zenith angles (SZA) less than 75° were used for the profile retrievals due to the large path lengths through the stratosphere for high SZA angles. This algorithm uses a two-step approach to determine the trace gas vertical profiles. In the first step, the aerosol profiles are retrieved using the measured O_4 DSCDs. A Monte Carlo approach is utilized to identify the best ensemble of the forward model parameters (column parameters (c) (VCD for trace gases and aerosol optical depth for aerosol), height parameter (h) and shape parameter (s)), which fit the measured O_4 DSCDs for the sequence of elevation angles. In the second step, the aerosol profiles retrieved from the O_4 inversion are used as an input to retrieve similar model parameters (c, h, and

s) for IO. The state of the atmosphere was calculated using the pressure and temperature profiles observed by the in-situ radiosondes, which were launched once a week at both stations. An angstrom exponent of 1 was used for the difference in the retrieval wavelengths as per observations made at Bharati in the past (Prakash Chaubey et al., 2011). Within MAPA, the differential air mass factors (AMFs) are calculated offline with the radiative transfer model McArtim (Deutschmann et al., 2011) for fixed nodes for each parameter and stored as a lookup table (LUT) for quick analysis. To assess the quality of the retrievals, MAPA provides "valid", "warning" or "error" flags for each measurement sequence, which are calculated based on pre-defined thresholds for various fit parameters. For further details about MAPA, please refer to the description paper by Beirle et al. (2018). Additionally, MAPA provides the option to use a scaling factor for significant mismatch between the modelled and measured O_4 DSCDs, which has been shown to be close to 0.8 in the past (Wagner et al., 2019). Using the variable option, where the model estimates the scaling factor, which ranged between 0.75 and 0.9. Therefore, a scaling factor of 0.8 was applied for all the campaigns.

We also make use of the IO vertical column densities retrieved using the SCanning Imaging Absorption spectroMeter for Atmospheric CHartographY (SCIAMACHY), a UV-vis-NIR spectrometer onboard the ENVISAT satellite (Burrows et al., 1995). Observations from SCIAMACHY stopped due to instrumental problems in April 2012. Here we make use of the mean from 2004-2011 to look at the geographical distribution and compare it with the ground-based observations made during the study period. Further details about the IO retrieval algorithm and the SCIAMACHY instrumental setup can be found elsewhere (Schönhardt et al., 2008, 2012).

3. Results and Discussion

3.1 Meteorological parameters

Figure 2 shows the 5-day back-trajectories arriving every hour at the two stations at a height of 10 m on the days that the DOAS measurements were conducted as a part of the three ISEA expeditions. The back-trajectories were calculated using the HYbrid Single-Particle Lagrangian Integrated Trajectory (HYSPLIT) using the using the EDAS-40 km database (Draxler and Rolph, 2003). The trajectories show that the airmasses sampled throughout the three expeditions were from either a remote oceanic region, coastal Antarctica, or the continental shelf. In general, most of the trajectories show that the airmasses had travelled over hundreds of kilometres over the last five days. For the local meteorological conditions, Figure 3 (top panels) show the wind direction at the Bharati station. Most of the time, the wind was from the ocean, with the winds coming from the north-west sector and a few instances of northern and north eastern winds (although during ISEA-34 the winds were mostly from east to north-east). This was during all the three expeditions at the Bharati station. The wind speed was mostly below 20 knots (~10 m s^{-1}) for all the campaigns, although periods of high winds were observed during ISEA-35 and ISEA-36, which were of a longer duration than ISEA-34. The temperature at the station hovered between -5 °C and +5 °C, through the summer period, with higher values closer to noon (Figure 3, middle panels). The humidity fluctuated from 40% to above 90%. The radiation followed a clear diurnal pattern, with the highest values seen around local noon and minima at local midnight. Considering that this region experiences continuous light for 24 hours, the radiation also showed a non-zero minima between November to January (Figure 3, bottom panels). However, in February, a clear night-time is seen in the radiation data. Finally, a measure of the cloudiness was also tracked using visual full sky cloud cover observations. Any cloud cover of more than 30% was considered to be cloudy

(cloud flag value of 1), which helps in filtering the MAX-DOAS observations. In addition to the visual inspection of the sky, which was performed once an hour, a second cloud index was calculated based on the ratios of the radiances at 320 nm and 440 nm from the 3° and zenith spectra (Mahajan et al., 2012; Wagner et al., 2014). Both manual and radiance-based indices showed a close match, indicating that cloudy conditions were well discerned by the cloud index calculation. Meteorological data was unfortunately not available at the Maitri station.

3.2 Differential Slant Column Densities (DSCDs)

Figure 4 shows the observed O_4 DSCDs at different elevation angles for all the campaigns. O_4 DSCDs were found to be higher at lower elevation angles, as expected, which is because the O_4 concentration is proportional to the square of the oxygen pressure and thus increases towards the surface. This also suggests that the aerosol loading was low in the atmosphere. Photons travel longer paths at lower elevation angles and interact more with tropospheric absorbing species before reaching the instrument resulting in a decreasing profile with increasing elevation angles. The average residual root mean square (RMS) and 2σ detection limit for the O_4 DSCDs were 4.46×10^{-4} (range: $1.56\text{-}10.01\times10^{-4}$) and 2.11×10^{42} molecules^2 cm^{-5} (range: $0.72\text{-}4.66 \times 10^{42}$ molecules^2 cm$^{-5)}$, respectively (Figure 4). The O_4 DSCDs were then used to estimate the aerosol profiles and hence the IO mixing ratios, as described earlier in section 2.

Figure 5 shows the observed IO DSCDs at different elevation angles for all the campaigns. The IO DSCDs were found to be higher at lower elevation angles, which indicates a decreasing gradient in the IO vertical profile. The residual RMS was in the $1.15\text{-}9.73\times10^{-4}$ range (mean: 3.46×10^{-4}), resulting in 2σ IO DSCD detection limits of 6.57×10^{12} to 5.71×10^{13} molecules cm^{-2} (mean 1.88×10^{13} molecules cm^{-2}) (Figure 5). For several days, only the lowermost elevation angles were

found to be above the two-sigma detection limit of the instrument. Higher IO DSCDs were observed at high SZAs, which is related to an increase in the path length. However, only observations with SZA<75° were used to estimate the vertical profiles and surface mixing ratios using the aerosol profiles derived using the O_4 DSCDs, as described earlier in section 2. A zoomed in view of two example days for both the O_4 and IO DSCDs is shown in Figure S2, which clearly shows the decreasing gradient with increasing elevation angles.

3.3 IO Vertical Column Densities (VCDs) and mixing ratio profiles

The O_4 and IO DSCDs were used to retrieve the vertical column densities and the vertical profiles for aerosols and IO. A comparison of the MAX-DOAS observed O_4 DSCDs with the MAPA modelled DSCDs for all the four campaigns are shown in Figure S3, and Figure S4 shows a similar plot for the IO DSCDs. Figure 6 and 7 show the MAPA calculated AODs and IO VCDs, respectively, for all the campaigns. Several datapoints are flagged as error or warnings, with a few scans giving a 'valid' flag. In the case of aerosols, the warning or error flags are mainly for scans which were during cloudy weather (Figure S5 shows the data, which were flagged as 'bad' and 'warning' along with the valid scans). As mentioned above, the cloud cover was regularly measured throughout the campaigns as a part of the meteorological observations. In addition to visual observations, we also computed the cloud index following past works based on MAX-DOAS observations (Mahajan et al., 2012; Wagner et al., 2014), which confirmed that the error and warning flags were during cloud cover periods. For the valid scans, the aerosol optical depth (AOD) ranged between 0.002 and 0.016, with a mean value of 0.003 for ISEA-34 at Bharati; between 0.001 and 0.067, with a mean value of 0.011 for ISEA-34 at Maitri; between 0.001 and 1.866, with a mean value of 0.037 for ISEA-35 at Bharati; and between 0.001 and 0.878, with a mean value of 0.016 for ISEA-36 at Bharati (Figure 6). The low values are expected considering

the pristine conditions in Antarctica, although during a couple of scans elevated levels were observed as demonstrated by the maximum value during ISEA-35 and ISEA-36. In the case of IO, there were far fewer valid retrieved profiles as can be seen in Figure 7 (Figure S6 shows the all scans, including the 'bad' and 'warning'). Only 343 valid total scans were retrieved for the vertical profiles of IO. One of the main reasons is that for most of the scans the IO DSCDs at higher elevation angles are below the detection limit and not enough information is available for the model to retrieve a valid vertical profile. In the case of IO VCDs, there were only two scans that showed a valid flag over the 10-day period during the ISEA-34 campaign at Bharati due to adverse weather conditions leading to mostly cloudy weather. Thus, the mean VCD value of 2.83×10^{12} molecules cm^{-2}, should be treated with some caution. In Maitri during ISEA-34, the IO VCD ranged between 2.37×10^{12} molecules cm^{-2} and 4.25×10^{12} molecules cm^{-2}, with a mean value of $3.40 \pm 0.57\times10^{12}$ molecules cm^{-2}. During ISEA-35 at Bharati, which had the highest number of valid scans over the four campaigns, the IO VCDs ranged between 0.01×10^{12} and 5.86×10^{12} molecules cm^{-2}, with a mean value of $2.62 \pm 1.16\times10^{12}$ molecules cm^{-2}. During ISEA-36, the IO VCDs ranged between 2.78×10^{12} molecules cm^{-2} and 4.90×10^{12} molecules cm^{-2}, with a mean value of $3.92 \pm 0.79\times10^{12}$ molecules cm^{-2} at Bharati.

In addition to the VCDs, vertical profiles of aerosols (Figure S7) and IO were estimated using MAPA. Figure 8 shows the typical vertical profiles of IO mixing ratios over the four expeditions. The surface mixing ratios for the valid scans across all the campaigns range between 0.2 and 1.3 pptv. The surface (<30 m) concentrations observed at both Maitri and Bharati are lower than observations in the Weddell Sea region, where summer time concentrations exceeding 6 pptv have been reported in the past (Atkinson et al., 2012; Saiz-Lopez et al., 2007a), or at the Neumayer station, where long-term zenith sky DOAS measurements of IO suggest mixing ratios as high as

~10 pptv during the summer (Frieß et al., 2001). It should be noted that although elevated concentrations were observed at Halley, the average summer concentration, measured only 4 m above the snowpack using a Long-Path DOAS instrument, was about 3 pptv, approximately a factor of three higher than the observations at Bharati and Maitri. Considering that the MAX-DOAS retrieved profiles are not very sensitive to the lowermost few meters, this difference is expected. This is because the source of IO is expected to be from the surface and remote sensing estimates have suggested that high IO concentrations in the order of 50 ppbv are present in the snow interstitial air (Frieß et al., 2010), suggesting that snowpack is indeed the source for iodine compounds. If this is the case, a strong gradient would be observed considering the short lifetime of IO in the atmosphere, and hence the MAX-DOAS observations would be lower than the LP-DOAS observations. However, this does not explain the large difference compared to Neumayer, where the estimated value was 10 pptv. Indeed, Maitri is close to Neumayer, and the reasons for the large difference between the two sites remains a mystery. The observations reported in this study are also similar to measurements at McMurdo Sound, near the Ross Sea, where MAX-DOAS observations reported a maximum of 2.6 ± 0.1 pptv with most of the observations below 1 pptv during 2006 and 2007 (Hay, 2010). It should be noted that the surface values were not highly weighted by the a priori. McMurdo Sound is also located in the East Antarctic, which shows lower levels of IO in the satellite estimates (Schönhardt et al., 2008) and in models (Fernandez et al., 2019).

Vertical profiles of IO have been reported only once in the past from Antarctica. These measurements were made at McMurdo Sound in East Antarctica (Hay, 2010). IO over two days in 2006 and 2007 show typical surface concentrations of ~1 pptv (with a maximum of 2.6 pptv), decreasing to ~0.2 pptv at about 200 m. A second maximum of 0.6 pptv at ~700 m was also

observed, but the models do not reproduce this profile shape and the observations were subject to large uncertainties with the vertical profile above 200 m dominated by the a priori (Hay, 2010). During the four campaigns studied here, elevated concentrations, similar to the surface, were usually observed until about 400 m. Above this height, there is a decrease, with the retrievals reducing to below 0.1 pptv (Figure 8). The reducing standard deviations in the profile retrieval with altitude show that all the profiles which reproduce elevated IO close to the ground approach zero for higher altitudes, suggesting that most of the IO is within the lower part of the troposphere. However, this gradient is much more gradual than estimates predicted using the THAMO one-dimensional model at Halley Bay (Saiz-Lopez et al., 2008). In most models, the assumption is that the source is from the snowpack, and hence a strong decreasing gradient with altitude has been predicted (Saiz-Lopez et al., 2008). The gradient of this decrease depends on the photolysis of the higher oxides, and on the recycling of iodine reservoir species on aerosols, both of which have uncertainties. When the gradient was estimated in 2008 (Saiz-Lopez et al., 2008), the photolysis rates for the higher iodine oxides were not available but this has recently been measured in the laboratory (Lewis et al., 2020) and THAMO needs to be updated accordingly. Another important point to consider is that the MAX-DOAS observation-based profile retrievals typically get only a couple of points of information in the boundary layer and are hence not expected to capture this strong decrease.

3.4 Comparison with satellite-based estimates

The satellite-based vertical column densities of IO across the Weddell Sea region, and the region encompassing Bharati and Maitri are shown in Figure 9. The averaged satellite based VCD observations suggest that lower levels of IO are expected at both the Indian bases as compared to places where ground-based observations have been reported in the past, such as Halley Bay and

Neumayer. The mean and standard deviation over the eight years of observations for Bharati is 0.6 ± 0.5 $\times 10^{12}$ molecules cm^{-2}, while for Maitri the amount is 0.5 ± 0.5 $\times 10^{12}$ molecules cm^{-2}, each for the whole time series. For single months the values can be higher: the mean IO VCD for Bharati is 0.8 or 0.4 $\times 10^{12}$ molecules cm^{-2} in December or February, respectively, and 0.6 $\times 10^{12}$ molecules cm^{-2} in March for Maitri. This is lower than mean value of 2.62 ± 1.16$\times 10^{12}$ molecules cm^{-2} observed at Bharati during ISEA-35, which was the longest dataset available in this study which suggests that the ground-based instruments observe larger VCDs as compared to the satellite based instruments. However, it should be noted that the SCIAMACHY data is an average over all the seasons, and individual daily datapoints as high as 2.1$\times 10^{12}$ molecules cm^{-2} have been observed. Figure 10 shows the timeseries for Bharati and Maitri with daily averages (red dots) as well as monthly averages (blue triangles) for the years 2004 to 2011. Satellite measurements from within 500 km around the stations were included in the analysis. It should be mentioned that this spatial averaging could cause introduction of larger uncertainties due to the heterogeneity in the IO distribution, but are necessary to improve the signal to noise.

When the whole IO column is constrained to the lower 400 m, the satellite retrieved VCDs translate to a range between 0.6 – 1.3 pptv. The daily satellite VCDs tend to exceed these averaged values and result in mixing ratios as high as 2 pptv. This is similar to the range observed through the four campaigns reported here. However, observations during the spring time were not made over these four campaigns, when emissions of iodine species have been show to peak at Halley Bay (Saiz-Lopez et al., 2007a). During the spring season, values as high as 20 pptv was observed at Halley Bay, a factor of ten higher than during the summer at the Indian stations. However, the satellite observations do not show a large peak over the springtime over both Indian stations. Another outstanding question is whether the satellites are sensitive to the lower 100-200 m, considering the

strong gradient in IO. Figure S8 shows the block AMFs for satellite retrievals showing a significant difference between the block AMFs over Antarctica at different albedo values. Over the ice-covered regions in Antarctica, the satellite is sensitive to the lower troposphere as the albedo is usually 0.9 or above. Observations have shown that open water has an albedo of 0.05–0.2 (Jin et al., 2004), whereas the albedo of sea ice ranges between 0.6 and 0.7 for bare ice and 0.8–0.9 for snow-covered ice (Perovich et al., 2002). In the case of Bharati, the Quilty Bay is not ice covered during the summer and hence along the light path in Bharati, the sensitivity of the satellite is much lower. Use of a higher albedo would result in an underestimation of the VCD by the satellite, which is the case when compared to the ground-based instruments. At Mairti this should not be the case considering that Maitri is 125 km inland from the coast, and the ice shelf is less than 1 km from the station along the light path. It should be noted that the MAPA LUTs are calculated for a low surface albedo (5%) and hence, at least for some of the measurements, the surface albedo is probably much higher, especially at Maitri. As far as we understand, the effect of the surface albedo mainly cancels out in the MAX-DOAS analysis, but it could be one possible uncertainty on the retrieval results. Another reason for the discrepancy between the ground based and satellite retrieved VCDs could be the overpass time, which was approximately 09:00 am local time. Although this should not be a large factor during the summer months due to long sunlit hours, and that the numbers given above were averages through the entire campaign for the ground-based observations, measurements at Halley Bay have shown a strong diurnal profile peaking at noon (Saiz-Lopez et al., 2007a). Hence, it is possible that the ground-based observations, which are filtered for SZA>75°, capture higher values than the satellite.

Finally, a point to consider is that the satellite data available from SCIAMACHY is for the period of 2004-2011, whereas the MAX-DOAS observations were conducted over three summers from

2015. This temporal discrepancy, although small considering the long satellite dataset, could contribute to the difference in the retrieved VCDs. Recent observations of iodine in ice-cores in the Alpine region and over Greenland have shown an increasing trend for atmospheric iodine in the northern hemisphere (Cuevas et al., 2018; Legrand et al., 2018). In the Antarctic only seasonal and geographical variations in halogens in the ice have been studied and no long term dataset is available (Vallelonga et al., 2017). The main cause for this increase is suggested to be an increase in tropospheric ozone, which drives the emission of iodine compounds from the ocean surface through heterogenous chemistry at the ocean interstitial surface (Carpenter et al., 2013). Although questions regarding the strength of this inorganic source in affecting IO concentrations in the Southern Ocean remain (Inamdar et al., 2020; Mahajan et al., 2019), it is possible that the discrepancy between the satellite and ground based data is because of a different time period. However, no increasing trend was observed in the satellite data for the period between 2004-2011 (Figure 10), which suggests that a factor of three increase in the VCDs is most likely due to a difference in the measurement technique and sensitivities rather than a change in the emissions.

3.5 Airmass origin dependence

Year-long observations at Halley Bay in West Antarctica, which were made using the LP-DOAS instrument, suggested a oceanic primary source (Saiz-Lopez et al., 2007a). The authors showed through the tracking of airmass back-trajectories, which displayed that elevated levels of IO were present in airmasses that passed over the coastal and oceanic regions compared to the airmasses that had only continental exposures. However, even in airmasses that had passed only over the continent for the past five days, the IO levels were still above the detection limit, which suggested

that even if the primary source is oceanic, a secondary source from the snow pack contributed to the atmospheric IO. Indeed, subsequent studies have tried to explain the snowpack source through recycling of primary emissions from the ocean (Fernandez et al., 2019) and one study has even suggested a strong snowpack source based on simulated observations (Frieß et al., 2010). Although the levels of IO are much lower than the peak concentrations seen at Halley Bay, we studied the back-trajectories to see if the origin of airmasses lead to a difference in the observed IO levels at both Bharati and Maitri. Considering the short lifetime of reactive iodine compounds in the atmosphere, we calculated the exposure of each HYSPLIT calculated back-trajectory according to the region it passed over the last 12 hours. Depending on where the trajectories spend the most amount of time, they were classified into coastal, continental, and oceanic airmasses. The coastal region was defined as a 0.5° belt along the Antarctic coastline, with regions to the north and south of this belt considered to be oceanic and continental, even though most of them had coastal origin when the 5 day trajectories are considered (Figure S9). Using the profiles which were valid, no clear dependence on the airmass origin was observed. Indeed, most of the data points at both stations corresponded to airmasses which were either coastal or continental (Figure S10) and is representative of the typical wind patterns during the summer season. Thus, using this dataset, it was not possible to draw any conclusions regarding the possible sources of IO in this region, and a longer study is needed in the future.

4. Conclusions

This study presents observations of iodine oxide (IO) at the Indian Antarctic bases Maitri and Bharati made over three summers from 2015 through 2017. IO was observed intermittently during

all the campaigns, with mixing ratios below 2 pptv. Using a profile retrieval algorithm, vertical gradients of IO were estimated, and these showed a decreasing profile with a peak in the boundary layer. The vertical profiles confirmed past hypothesis of a source from the ground considering a sharp gradient. The vertical columns observed using the ground-based instrument are approximately a factor of three-five higher than the climatological mean observed by the satellite, which could be due to a difference in the measurement techniques and sensitivities. Airmass origin analysis using back-trajectories did not lead to a conclusive answer about the source regions. Indeed, it raises new questions on comparison with past observations, which show that we still do not understand iodine chemistry in the polar regions. This study suggests that a longer dataset over different seasons and regions of Antarctica is necessary to answer the outstanding questions regarding the sources and seasonal importance of IO in the Indian Ocean sector of Antarctica.

5. Acknowledgements

We thank the logistical and scientific teams of the ISEA-34, ISEA-35, and ISEA-36 campaigns for enabling observations through the expeditions. The ISEA campaigns are organised by the National Centre for Polar and Ocean Research (NCPOR), Ministry of Earth Sciences (MOES), Government of India. IITM and NCPOR are funded by MOES, Government of India.

6. Author contributions:

ASM conceptualised the research plan and methodology, did the analysis and wrote the manuscript. MSB did the field observations. SB, TW, NB and ASL helped with the interpretation of the observations and AS provided the satellite observations and helped interpret them.

7. References

Allan, J. D., Williams, P. I., Najera, J., Whitehead, J. D., Flynn, M. J., Taylor, J. W., Liu, D., Darbyshire, E., Carpenter, L. J., Chance, R., Andrews, S. J., Hackenberg, S. C. and McFiggans, G.: Iodine observed in new particle formation events in the Arctic atmosphere during ACCACIA, Atmos. Chem. Phys., 15(10), 5599–5609, doi:10.5194/acp-15-5599-2015, 2015.

Atkinson, H. M., Huang, R.-J., Chance, R., Roscoe, H. K., Hughes, C., Davison, B., Schönhardt, A., Mahajan, A. S., Saiz-Lopez, A., Hoffmann, T. and Liss, P. S.: Iodine emissions from the sea ice of the Weddell Sea, Atmos. Chem. Phys., 12, 11229–11244, doi:10.5194/acp-12-11229-2012, 2012.

Barrie, L. A., Bottenheim, J. W., Schnell, R. C., Crutzen, P. J. and Rasmussen, R. A.: Ozone destruction and photochemical reactions at polar sunrise in the lower Arctic atmosphere, Nature, 334(14), 138–141 [online] Available from: http://www.nature.com/nature/journal/v334/n6178/abs/334138a0.html (Accessed 3 May 2012), 1988.

Beirle, S., Dörner, S., Donner, S., Remmers, J., Wang, Y. and Wagner, T.: The Mainz Profile Algorithm (MAPA), Atmos. Meas. Tech. Discuss., 1–33, doi:10.5194/amt-2018-375, 2018.

Bogumil, K., Orphal, J., Homann, T., Voigt, S., Spietz, P., Fleischmann, O. C., Vogel, A., Hartmann, M., Kromminga, H., Bovensmann, H., Frerick, J. and Burrows, J. P.: Measurements of molecular absorption spectra with the SCIAMACHY pre-flight model: instrument characterization and reference data for atmospheric remote-sensing in the 230–2380 nm region, J. Photochem. Photobiol. A Chem., 157(2–3), 167–184, doi:10.1016/S1010-6030(03)00062-5, 2003.

Bottenheim, J. W., Gallant, A. G. and Brice, K. A.: Measurements of NOy Species and O3 at 82-Degrees-N Latitude, Geophys. Res. Lett., 13(2), 113–116, 1986.

Burrows, J. P., Hölzle, E., Goede, A. P. H., Visser, H. and Fricke, W.: SCIAMACHY – Scanning Imaging Absorption Spectrometer for Atmospheric Chartography, Acta Astronaut., 35, 445–451, 1995.

Buys, Z., Brough, N., Huey, L. G., Tanner, D. J., von Glasow, R. and Jones, a. E.: High temporal resolution Br2, BrCl and BrO observations in coastal Antarctica, Atmos. Chem. Phys., 13, 1329–1343, doi:10.5194/acp-13-1329-2013, 2013.

Carpenter, L. J., Wevill, D. J., Palmer, C. J. and Michels, J.: Depth profiles of volatile iodine and bromine-containing halocarbons in coastal Antarctic waters, Mar. Chem., 103, 227–236, 2007.

Carpenter, L. J., MacDonald, S. M., Shaw, M. D., Kumar, R., Saunders, R. W., Parthipan, R., Wilson, J. and Plane, J. M. C.: Atmospheric iodine levels influenced by sea surface emissions of inorganic iodine, Nat. Geosci., 6(2), 108–111, doi:10.1038/ngeo1687, 2013.

Chance, K. V and Spurr, R. J.: Ring effect studies: Rayleigh scattering, including molecular parameters for rotational Raman scattering, and the Fraunhofer spectrum., Appl. Opt., 36(21), 5224–5230 [online] Available from: http://www.ncbi.nlm.nih.gov/pubmed/18259337, 1997.

Cuevas, C. A., Maffezzoli, N., Corella, J. P., Spolaor, A., Vallelonga, P., Kjær, H. A., Simonsen, M., Winstrup, M., Vinther, B., Horvat, C., Fernandez, R. P., Kinnison, D., Lamarque, J.-F., Barbante, C. and Saiz-Lopez, A.: Rapid increase in atmospheric iodine levels in the North Atlantic since the mid-20th century, Nat. Commun., 9(1), 1452, doi:10.1038/s41467-018-03756-1, 2018.

Deutschmann, T., Beirle, S., Frieß, U., Grzegorski, M., Kern, C., Kritten, L., Platt, U., Prados-Román, C., Pukite, J., Wagner, T., Werner, B. and Pfeilsticker, K.: The Monte Carlo atmospheric radiative transfer model McArtim: Introduction and validation of Jacobians and 3D features, J. Quant. Spectrosc. Radiat. Transf., 112(6), 1119–1137, doi:10.1016/j.jqsrt.2010.12.009, 2011.

Draxler, R. and Rolph, G.: HYSPLIT (HYbrid Single Particle Lagrangian Integrated Trajectory). Model access via NOAA ARL Ready, [online] Available from: http://www.arl.noaa.gov/ready/ hysplit4.html, 2003.

Fayt, C. and Van Roozendael, M.: QDOAS 1.00. Software User Manual, [online] Available from: http://uv-vis.aeronomie.be/software/QDOAS/, 2013.

Fernandez, R. P., Carmona-Balea, A., Cuevas, C. A., Barrera, J. A., Kinnison, D. E., Lamarque, J., Blaszczak-Boxe, C., Kim, K., Choi, W., Hay, T., Blechschmidt, A., Schönhardt, A., Burrows, J. P. and Saiz-Lopez, A.: Modeling the Sources and Chemistry of Polar Tropospheric Halogens (Cl, Br, and I) Using the CAM-Chem Global Chemistry-Climate Model, J. Adv. Model. Earth Syst., 11(7), 2259–2289, doi:10.1029/2019MS001655, 2019.

Fogelqvist, E. and Tanhua, T.: Iodinated C1-C4 hydrocarbons released from ice algae in Antarctica BT - Naturally-Produced Organohalogens, edited by A. Grimvall and E. W. B. de Leer, pp. 295–305, Springer Netherlands, Dordrecht., 1995.

Frieß, U., Wagner, T., Pundt, I., Pfeilsticker, K., Platt, U. and Friefi, U.: Spectroscopic Measurements of Tropospheric Iodine Oxide at Neumayer Station, Antarctica, Geophys. Res. Lett., 28(10), 1941–1944, 2001.

Frieß, U., Deutschmann, T., Gilfedder, B. S., Weller, R. and Platt, U.: Iodine monoxide in the

506 Antarctic snowpack, Atmos. Chem. Phys., 10(5), 2439–2456 [online] Available from:
507 http://www.atmos-chem-phys.net/10/2439/2010/, 2010.

508 Garrison, D. L. and Buck, K. R.: The biota of Antarctic pack ice in the Weddell sea and
509 Antarctic Peninsula regions, Polar Biol., 10(3), 211–219, doi:10.1007/BF00238497, 1989.

510 Gómez Martín, J. C., Spietz, P. and Burrows, J. P.: Spectroscopic studies of the I-2/O-3
511 photochemistry - Part 1: Determination of the absolute absorption cross sections of iodine oxides
512 of atmospheric relevance, J. Photochem. Photobiol. A - Chem., 176(1–3), 15–38,
513 doi:10.1016/j.jphotochem.2005.09.024, 2005.

514 Grilli, R., Legrand, M., Kukui, A., Méjean, G., Preunkert, S. and Romanini, D.: First
515 investigations of IO, BrO, and NO2 summer atmospheric levels at a coastal East Antarctic site
516 using mode-locked cavity enhanced absorption spectroscopy., Geophys. Res. Lett., 40(4), 791–
517 796, doi:10.1002/GRL.50154, 2013.

518 Hay, T.: MAX – DOAS measurements of bromine explosion events in McMurdo Sound ,
519 Antarctica, University of Canterbury., 2010.

520 Hollwedel, J., Wenig, M., Beirle, S., Kraus, S., Kühl, S., Wilms-Grabe, W., Platt, U. and
521 Wagner, T.: Year-to- Year Variability of Polar Tropospheric BrO as seen by GOME, Adv. Sp.
522 Res., 34, 804–808 [online] Available from: http://dx.doi.org/10.1016/j.asr.2003.08.060, 2004.

523 Hönninger, G., von Friedeburg, C. and Platt, U.: Multi axis differential optical absorption
524 spectroscopy (MAX-DOAS), Atmos. Chem. Phys., 4, 231–254, doi:10.5194/acp-4-231-2004,
525 2004.

526 Inamdar, S., Tinel, L., Chance, R., Carpenter, L. J., Sabu, P., Chacko, R., Tripathy, S. C., Kerkar,

A. U., Sinha, A. K., Bhaskar, P. V., Sarkar, A., Roy, R., Sherwen, T. T., Cuevas, C., Saiz-Lopez, A., Ram, K. and Mahajan, A. S.: Estimation of Reactive Inorganic Iodine Fluxes in the Indian and Southern Ocean Marine Boundary Layer, Atmos. Chem. Phys., 20(20), 12093–12114, doi:10.5194/acp-20-12093-2020, 2020.

Jin, Z., Charlock, T. P., Smith, W. L. and Rutledge, K.: A parameterization of ocean surface albedo, Geophys. Res. Lett., 31(22), 1–4, doi:10.1029/2004GL021180, 2004.

Koenig, T. K., Baidar, S., Campuzano-Jost, P., Cuevas, C. A., Dix, B., Fernandez, R. P., Guo, H., Hall, S. R., Kinnison, D., Nault, B. A., Ullmann, K., Jimenez, J. L., Saiz-Lopez, A. and Volkamer, R.: Quantitative detection of iodine in the stratosphere, Proc. Natl. Acad. Sci., (15), 201916828, doi:10.1073/pnas.1916828117, 2020.

Kreher, K., Johnston, P. V., Wood, S. W., Nardi, B. and Platt, U.: Ground-based measurements of tropospheric and stratospheric BrO at Arrival Heights, Antarctica, Geophys. Res. Lett., 24(23), 3021–3024, doi:10.1029/97GL02997, 1997.

Legrand, M., McConnell, J. R., Preunkert, S., Arienzo, M., Chellman, N., Gleason, K., Sherwen, T., Evans, M. J. and Carpenter, L. J.: Alpine ice evidence of a three-fold increase in atmospheric iodine deposition since 1950 in Europe due to increasing oceanic emissions, Proc. Natl. Acad. Sci., 115(48), 12136–12141, doi:10.1073/pnas.1809867115, 2018.

Lewis, T. R., Gómez Martín, J. C., Blitz, M. A., Cuevas, C. A., Plane, J. M. C. and Saiz-Lopez, A.: Determination of the absorption cross sections of higher-order iodine oxides at 355 and 532 nm, Atmos. Chem. Phys., 20(18), 10865–10887, doi:10.5194/acp-20-10865-2020, 2020.

Mahajan, A. S., Shaw, M., Oetjen, H., Hornsby, K. E., Carpenter, L. J., Kaleschke, L., Tian-

548 Kunze, X., Lee, J. D., Moller, S. J., Edwards, P. M., Commane, R., Ingham, T., Heard, D. E. and
549 Plane, J. M. C.: Evidence of reactive iodine chemistry in the Arctic boundary layer, J. Geophys.
550 Res., 115(D20303,), doi:dx.doi.org/10.1029/2009JD013665, 2010.

551 Mahajan, A. S., Gómez Martín, J. C., Hay, T. D., Royer, S.-J., Yvon-Lewis, S. A., Liu, Y., Hu,
552 L., Prados-Román, C., Ordóñez, C., Plane, J. M. C. and Saiz-Lopez, A.: Latitudinal distribution
553 of reactive iodine in the Eastern Pacific and its link to open ocean sources, Atmos. Chem. Phys.,
554 12, 11609–11617, doi:10.5194/acp-12-11609-2012, 2012.

555 Mahajan, A. S., Tinel, L., Hulswar, S., Cuevas, C. A., Wang, S., Ghude, S., Naik, R. K., Mishra,
556 R. K., Sabu, P., Sarkar, A., Anilkumar, N. and Saiz Lopez, A.: Observations of iodine oxide in
557 the Indian Ocean marine boundary layer: A transect from the tropics to the high latitudes, Atmos.
558 Environ. X, 1, 100016, doi:10.1016/j.aeaoa.2019.100016, 2019.

559 Meller, R. and Moortgat, G. K.: Temperature dependence of the absorption cross sections of
560 formaldehyde between 223 and 323 K in the wavelength range 225-375 nm, J. Geophys. Res.,
561 105(D6), 7089–7101 [online] Available from: http://dx.doi.org/10.1029/1999JD901074, 2000.

562 O'Dowd, C. D., Facchini, M. C., Cavalli, F., Ceburnis, D., Mircea, M., Decesari, S., Fuzzi, S.,
563 Yoon, Y. J., Putaud, J. P. and Dowd, C. D. O.: Biogenically driven organic contribution to
564 marine aerosol, Nature, 431(7009), 676–680, doi:10.1038/nature02970.1., 2004.

565 Oltmans, S. J. and Komhyr, W. D.: Surface Ozone Distributions and Variations from 1973-1984
566 Measurements at the Noaa Geophysical Monitoring for Climatic-Change Base-Line
567 Observatories, J. Geophys. Res. - Atmos., 91(D4), 5229–5236, 1986.

568 Perovich, D. K., Grenfell, T. C., Light, B. and Hobbs, P. V.: Seasonal evolution of the albedo of

multiyear Actic sea ice, J. Geophys. Res. C Ocean., 107(10), doi:10.1029/2000jc000438, 2002.

Platt, U. and Stutz, J.: Differential optical absorption spectroscopy: Principles and applications, First Edit., Springer., 2008.

Prakash Chaubey, J., Krishna Moorthy, K., Suresh Babu, S. and S. Nair, V.: The optical and physical properties of atmospheric aerosols over the Indian Antarctic stations during southern hemispheric summer of the International Polar Year 2007â€"2008, Ann. Geophys., 29(1), 109–121, doi:10.5194/angeo-29-109-2011, 2011.

Raso, A. R. W., Custard, K. D., May, N. W., Tanner, D., Newburn, M. K., Walker, L., Moore, R. J., Huey, L. G., Alexander, L., Shepson, P. B. and Pratt, K. A.: Active molecular iodine photochemistry in the Arctic, Proc. Natl. Acad. Sci. U. S. A., 114(38), 10053–10058, doi:10.1073/pnas.1702803114, 2017.

Reifenhäuser, W. and Heumann, K. G.: Determinations of methyl-iodine in the antarctic atmosphere at the south polar sea, Atmos. Environ. Part a-General Top., 26(16), 2905–2912, 1992.

Richter, A., Wittrock, F., Ladstätter-Weißenmayer, A. and Burrows, J. P.: GOME measurements of stratospheric and tropospheric BrO, Adv. Sp. Res., 29(11), 1667–1672, 2002.

Rothman, L. S., Gordon, I. E., Babikov, Y., Barbe, A., Chris Benner, D., Bernath, P. F., Birk, M., Bizzocchi, L., Boudon, V., Brown, L. R., Campargue, A., Chance, K., Cohen, E. a., Coudert, L. H., Devi, V. M., Drouin, B. J., Fayt, A., Flaud, J.-M., Gamache, R. R., Harrison, J. J., Hartmann, J.-M., Hill, C., Hodges, J. T., Jacquemart, D., Jolly, A., Lamouroux, J., Le Roy, R. J., Li, G., Long, D. a., Lyulin, O. M., Mackie, C. J., Massie, S. T., Mikhailenko, S., Müller, H. S. P.,

Naumenko, O. V., Nikitin, A. V., Orphal, J., Perevalov, V., Perrin, A., Polovtseva, E. R., Richard, C., Smith, M. a. H., Starikova, E., Sung, K., Tashkun, S., Tennyson, J., Toon, G. C., Tyuterev, V. G. and Wagner, G.: The HITRAN 2012 molecular spectroscopic database, J. Quant. Spectrosc. Radiat. Transf., 130, 4–50, doi:10.1016/j.jqsrt.2013.07.002, 2013.

Saiz-Lopez, A. and Blaszczak-boxe, C. S.: The polar iodine paradox, Atmos. Environ., 145, 72–73, doi:10.1016/j.atmosenv.2016.09.019, 2016.

Saiz-Lopez, A. and von Glasow, R.: Reactive halogen chemistry in the troposphere., Chem. Soc. Rev., doi:10.1039/c2cs35208g, 2012.

Saiz-Lopez, A., Mahajan, A. S., Salmon, R. A., Bauguitte, S. J.-B., Jones, A. E., Roscoe, H. K. and Plane, J. M. C.: Boundary Layer Halogens in Coastal Antarctica, Science (80-.)., 317(5836), 348–351, doi:10.1126/science.1141408, 2007a.

Saiz-Lopez, A., Chance, K. V., Liu, X., Kurosu, T. P. and Sander, S. P.: First observations of iodine oxide from space, Geophys. Res. Lett., 34(12), L12812, doi:10.1029/2007GL030111, 2007b.

Saiz-Lopez, A., Plane, J. M. C., Mahajan, A. S., Anderson, P. S., Bauguitte, S. J.-B., Jones, A. E., Roscoe, H. K., Salmon, R. A., Bloss, W. J., Lee, J. D. and Heard, D. E.: On the vertical distribution of boundary layer halogens over coastal Antarctica: implications for O-3, HOx, NOx and the Hg lifetime, Atmos. Chem. Phys., 8(4), 887–900, 2008.

Saiz-Lopez, A., Plane, J. M. C., Baker, A. R., Carpenter, L. J., von Glasow, R., Martín, J. C. G., McFiggans, G. B., Saunders, R. W. and Gómez Martín, J. C.: Atmospheric Chemistry of Iodine, Chem. Rev., 112(3), 1773–1804, doi:10.1021/cr200029u, 2012.

611 Saiz-Lopez, A., Blaszczak-Boxe, C. S. and Carpenter, L. J.: A mechanism for biologically-
612 induced iodine emissions from sea-ice, Atmos. Chem. Phys., 15, 9731–9746, doi::10.5194/acp-
613 15-9731-2015, 2015a.

614 Saiz-Lopez, A., Baidar, S., Cuevas, C. A., Koenig, T. K., Fernandez, R. P., Dix, B., Kinnison, D.
615 E., Lamarque, J., Rodriguez-Lloveras, X., Campos, T. L. and Volkamer, R.: Injection of iodine
616 to the stratosphere, Geophys. Res. Lett., 42, 6852–6859, doi:10.1002/2015GL064796, 2015b.

617 Schönhardt, A., Richter, A., Wittrock, F., Kirk, H., Oetjen, H., Roscoe, H. K. and Burrows, J. P.:
618 Observations of iodine monoxide (IO) columns from satellite, Atmos. Chem. Phys., 8, 637–653
619 [online] Available from: http://hal-insu.archives-ouvertes.fr/hal-00296438/ (Accessed 30 April
620 2012), 2008.

621 Schönhardt, A., Begoin, M., Richter, a., Wittrock, F., Kaleschke, L., Gómez Martín, J. C. and
622 Burrows, J. P.: Simultaneous satellite observations of IO and BrO over Antarctica, Atmos.
623 Chem. Phys., 12(14), 6565–6580, doi:10.5194/acp-12-6565-2012, 2012.

624 Stutz, J., Kim, E. S., Platt, U., Bruno, P., Perrino, C. and Febo, A.: UV-visible absorption cross
625 sections of nitrous acid, J. Geophys. Res., 105(D11), 14585–14592, 2000.

626 Thalman, R. and Volkamer, R. A.: Temperature Dependent Absorption Cross-Sections of O2-O2
627 collision pairs between 340 and 630 nm and at atmospherically relevant pressure, Phys. Chem.
628 Chem. Phys., 15, 15371–15381, doi:10.1039/C3CP50968K, 2013.

629 Theys, N., Van Roozendael, M., Hendrick, F., Yang, X., De Smedt, I., Richter, A., Begoin, M.,
630 Errera, Q., Johnston, P. V., Kreher, K. and De Mazière, M.: Global observations of tropospheric
631 BrO columns using GOME-2 satellite data, Atmos. Chem. Phys., 11, 1791–1811,

632 doi:10.5194/acp-11-1791-2011, 2011.

633 Tuckermann, M., Ackermann, R., Golz, C., LorenzenSchmidt, H., Senne, T., Stutz, J., Trost, B.,
634 Unold, W., Platt, U. and Lorenzen-Schmidt, H.: DOAS-observation of halogen radical-catalysed
635 arctic boundary layer ozone destruction during the ARCTOC-campaigns 1995 and 1996 in Ny-
636 Alesund, Spitsbergen, Tellus B, 49B(5), 533–555, 1997.

637 Vallelonga, P., Maffezzoli, N., Moy, A. D., Curran, M. A. J., Vance, T. R., Edwards, R., Hughes,
638 G., Barker, E., Spreen, G., Saiz-Lopez, A., Corella, J. P., Cuevas, C. A. and Spolaor, A.: Sea-ice-
639 related halogen enrichment at Law Dome, coastal East Antarctica, Clim. Past, 13(2), 171–184,
640 doi:10.5194/cp-13-171-2017, 2017.

641 Vandaele, A. C., Hermans, C., Simon, P., Carleer, M. R., Colins, R., Fally, F., Merienne, M. F.,
642 Jenouvrier, A. and Coquart, B.: Measurements of NO2 absorption cross-sections at 42000 cm-1
643 to 10000 cm-1 (238-1000 nm) at 220 K and 298 K, J. Quant. Spectrosc. Radiat. Transf., 59, 171–
644 184, 1997.

645 Vandaele, A. C., Hermans, C., Simon, P. C., Carleer, M., Colin, R., Fally, S., Merienne, M. F.,
646 Jenouvrier, A. and Coquartii, B.: Measurements od the NO2 absorption cross-section from 42000
647 cm-1 to 10000 cm-1 (238-1000 nm) at 220 K and 294 K, J. Quant. Spectrosc. Radiat. Transf.,
648 59(3), 171–184, 1998.

649 Wagner, T., Leue, C., Wenig, M., Pfeilsticker, K. and Platt, U.: Spatial and temporal distribution
650 of enhanced boundary layer BrO concentrations measured by the GOME instrument aboard
651 ERS-2, J. Geophys. Res. - Atmos., 106(D20), 24225–24235, 2001.

652 Wagner, T., Dix, B., Friedeburg, C. V., Frieß, U., Sanghavi, S., Sinreich, R. and Platt, U.: MAX-

DOAS O 4 measurements: A new technique to derive information on atmospheric aerosols—Principles and information content, J. Geophys. Res., 109(D22), doi:10.1029/2004JD004904, 2004.

Wagner, T., Beirle, S. and Deutschmann, T.: Three-dimensional simulation of the Ring effect in observations of scattered sun light using Monte Carlo radiative transfer models, Atmos. Meas. Tech., 2(1), 113–124, doi:10.5194/amt-2-113-2009, 2009.

Wagner, T., Apituley, A., Beirle, S., Dörner, S., Friess, U., Remmers, J. and Shaiganfar, R.: Cloud detection and classification based on MAX-DOAS observations, Atmos. Meas. Tech., 7(5), 1289–1320, doi:10.5194/amt-7-1289-2014, 2014.

Wagner, T., Beirle, S., Benavent, N., Bösch, T., Chan, K. L., Donner, S., Dörner, S., Fayt, C., Frieß, U., García-Nieto, D., Gielen, C., González-Bartolome, D., Gomez, L., Hendrick, F., Henzing, B., Jin, J. L., Lampel, J., Ma, J., Mies, K., Navarro, M., Peters, E., Pinardi, G., Puentedura, O., Puķīte, J., Remmers, J., Richter, A., Saiz-Lopez, A., Shaiganfar, R., Sihler, H., Van Roozendael, M., Wang, Y. and Yela, M.: Is a scaling factor required to obtain closure between measured and modelled atmospheric O₄ absorptions? An assessment of uncertainties of measurements and radiative transfer simulations for 2 selected days during th, Atmos. Meas. Tech., 12(5), 2745–2817, doi:10.5194/amt-12-2745-2019, 2019.

673 Figures

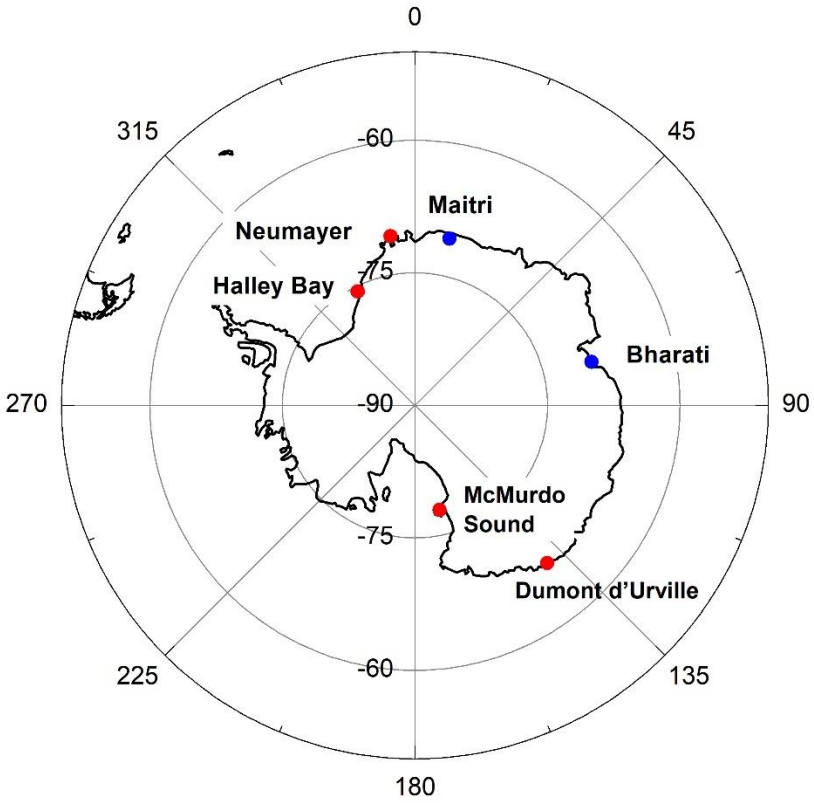

674

675 **Figure 1:** Map showing the location of the two Indian Antarctic stations, Maitri and Bharati, where
676 observations of IO were performed during this study (blue dots). Previous locations that have
677 reported observations of IO are also marked on the map (red dots).

678

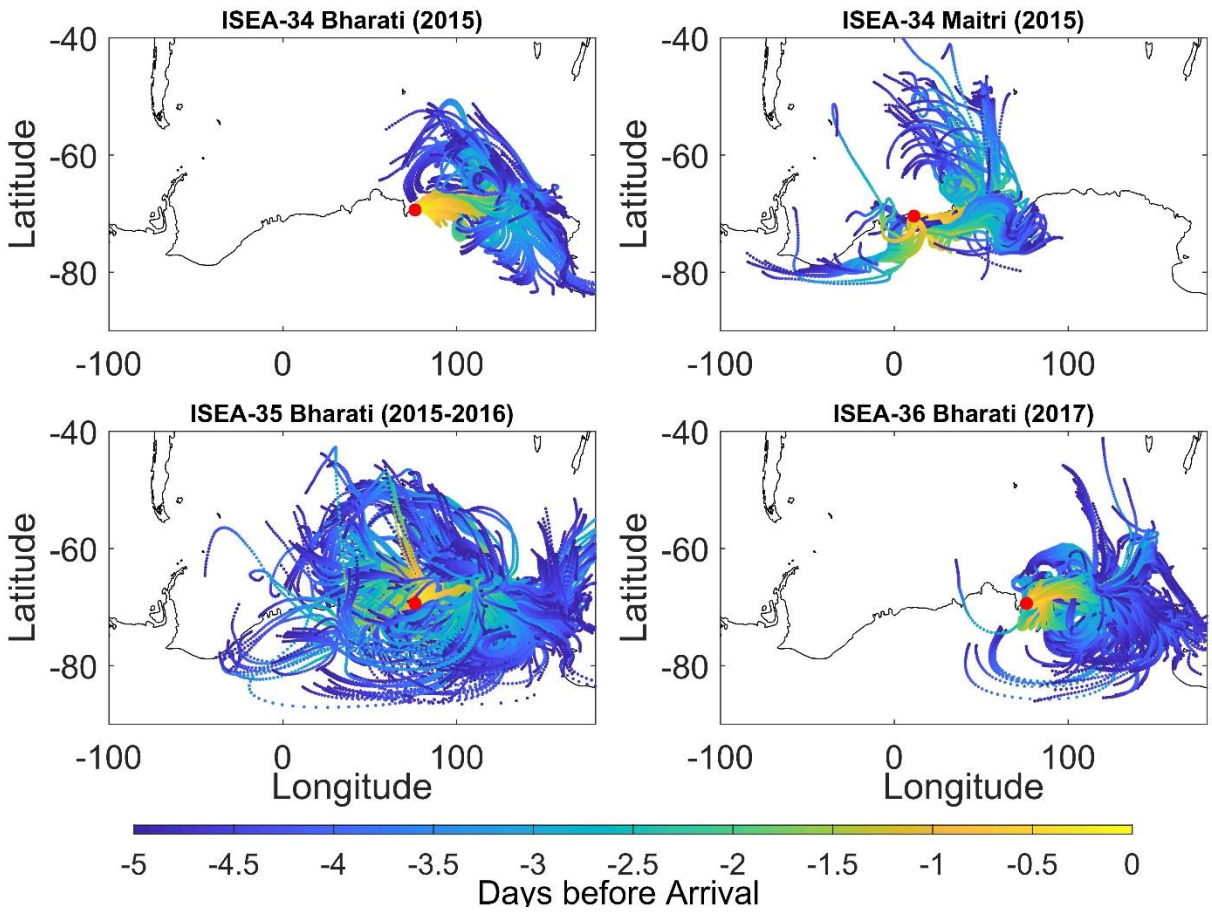

679

680 **Figure 2:** 5-day back-trajectories arriving at the two stations on the days that the measurements of
681 IO were conducted as a part of the 34th, 35th and 36th ISEA expeditions are shown. The back-
682 trajectories were calculated using the HYbrid Single-Particle Lagrangian Integrated Trajectory
683 (HYSPLIT) model, arriving every hour (Draxler and Rolph, 2003).

684

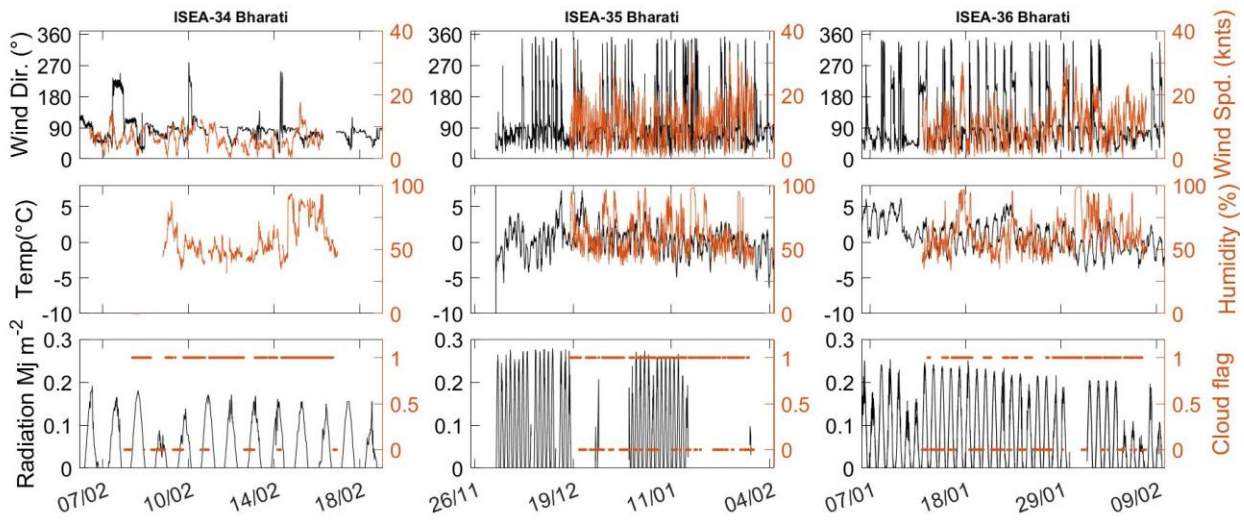

685

686 **Figure 3:** Observations of different meteorological parameters that were measured during the
687 various summer campaigns are shown here. The top panels show the wind direction and speed; the
688 middle panels show the temperature and humidity; and the bottom panels show the radiation and
689 cloudiness (1 is defined as 30% cloudy skies and above). Observations of these parameters were
690 not made during the 34th ISEA at Maitri and the gaps indicate instrumental or observational issues.
691 The data had a time resolution of 5 min.

692

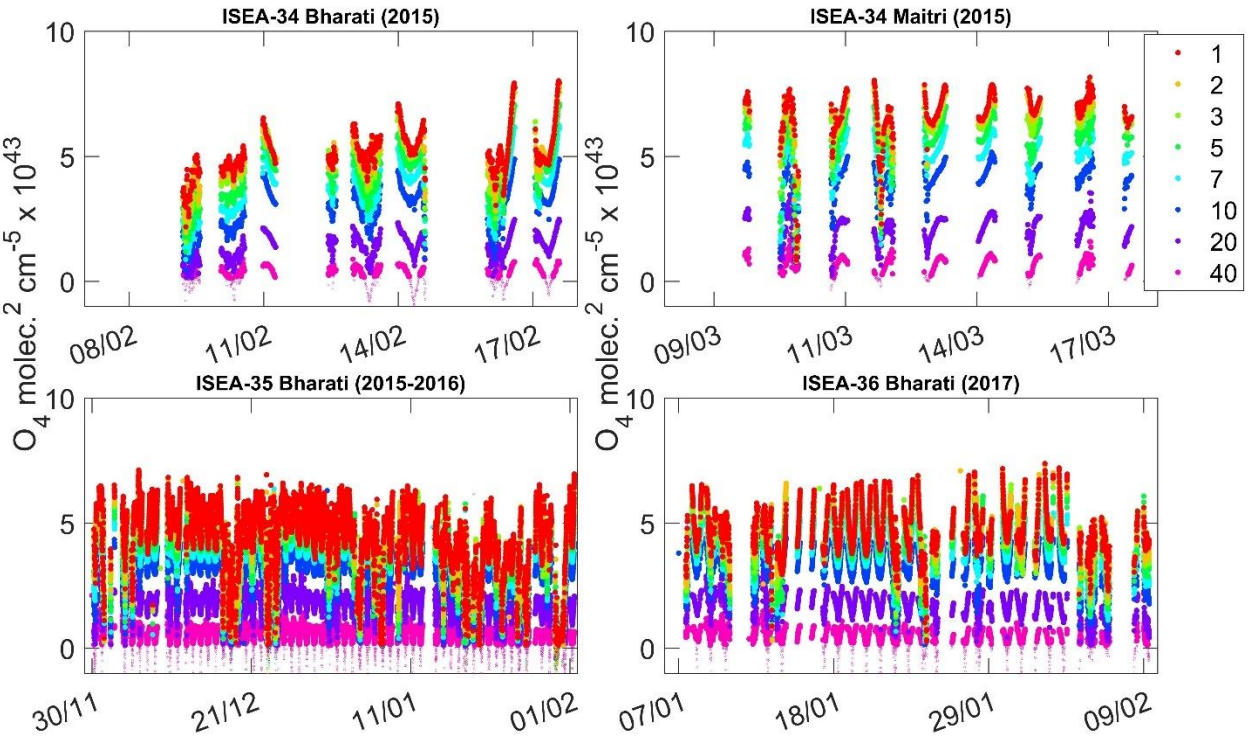

693

694 **Figure 4:** O_4 DSCDs observed during the four campaigns are shown. The empty circles represent

695 values below the 2σ detection limit of the instrument, while the filled circles are values above the

696 2σ detection limit. The data are color-coded according to elevation angles.

697

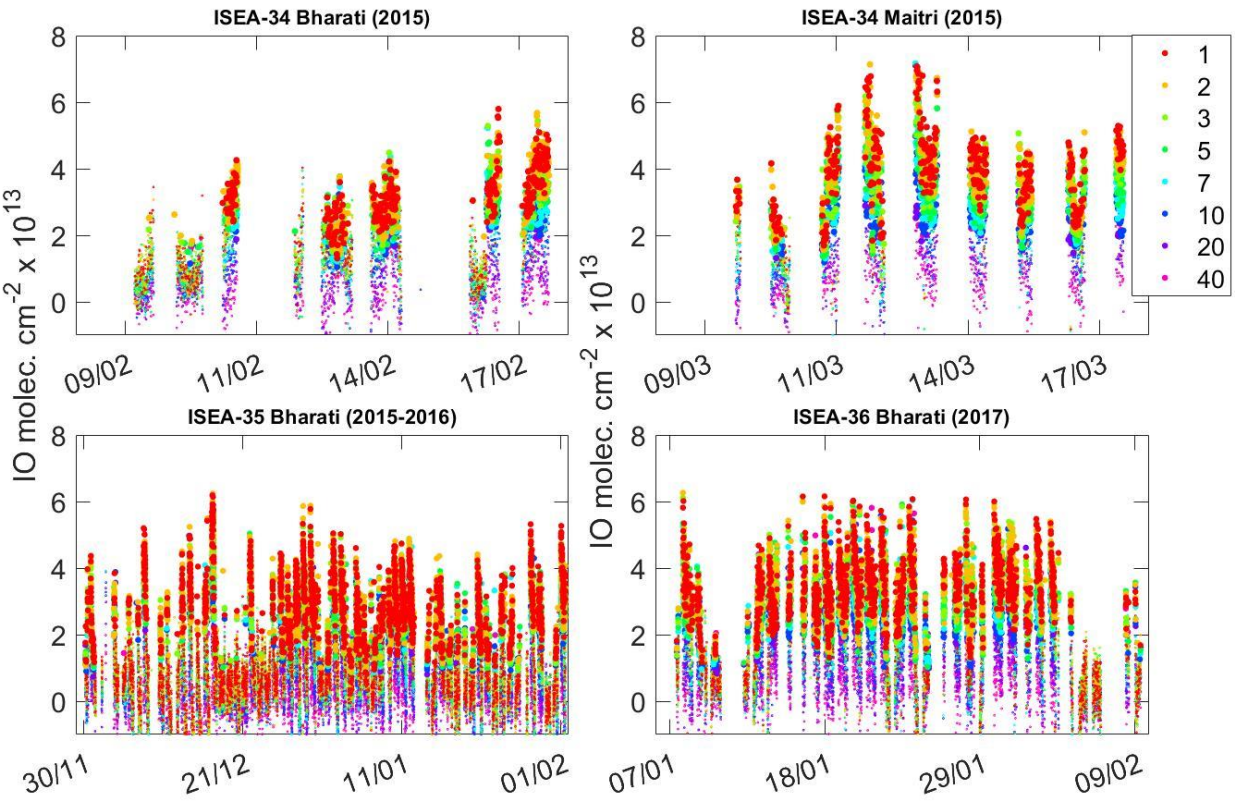

Figure 5: IO DSCDs observed during the four campaigns are shown. The smaller circles represent values below the 2σ detection limit of the instrument, while the bigger circles are values above the 2σ detection limit. The data are color-coded according to elevation angles.

703

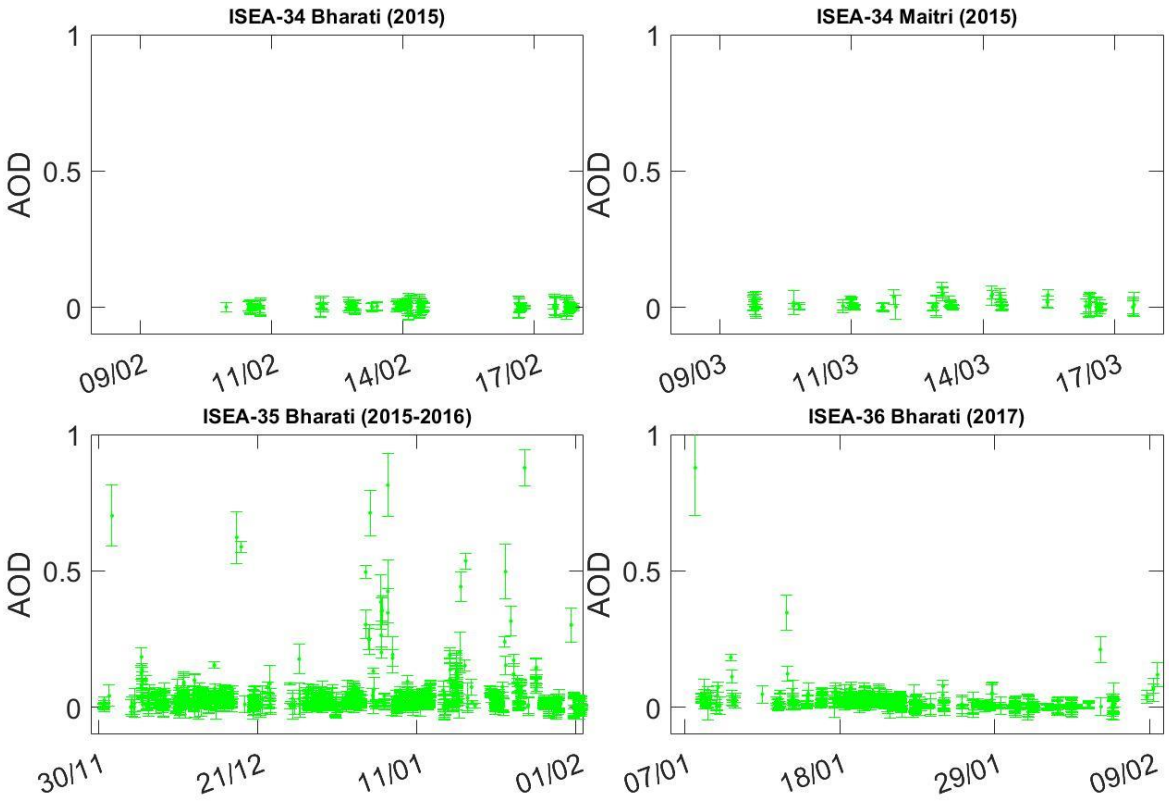

704

705 **Figure 6:** AOD timeseries retrieved using the O_4 DSCDs for all the four campaigns are shown.
706 The data show only the 'good' datapoints, which are reliable and were mostly during clear sky
707 conditions.

708

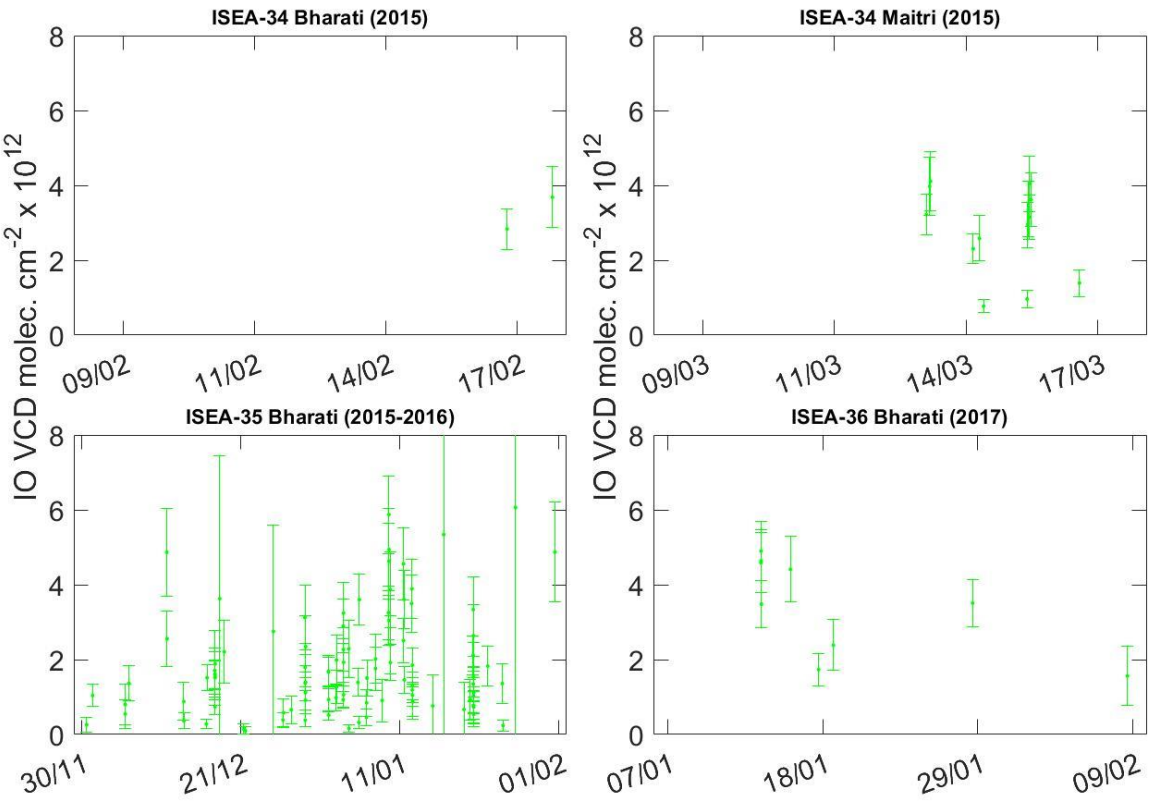

709

710 **Figure 7:** Observations of IO vertical column densities observed through all the four campaigns
711 are shown. These data were mostly during periods of clear sky, and where IO was observed above
712 the detection limit for most of the set elevation angles, enabling a reliable profile retrieval.

713

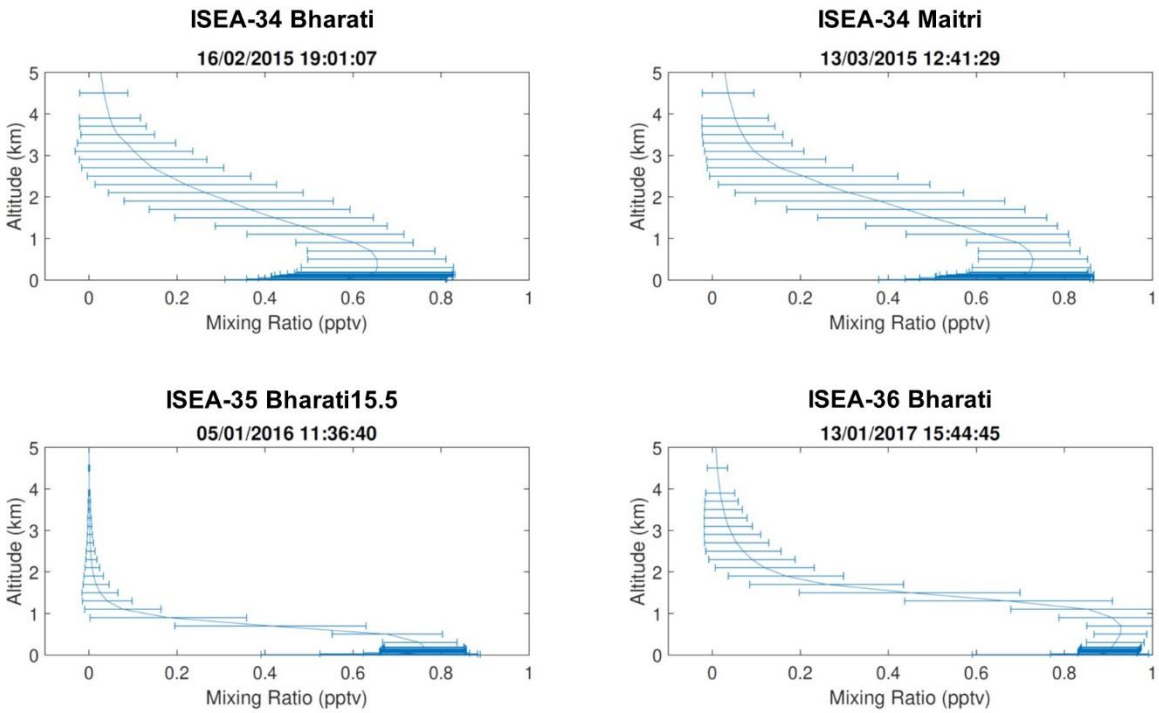

714

715 **Figure 8:** Typical examples of IO vertical profiles retrieved during all the four campaigns are

716 shown.

717

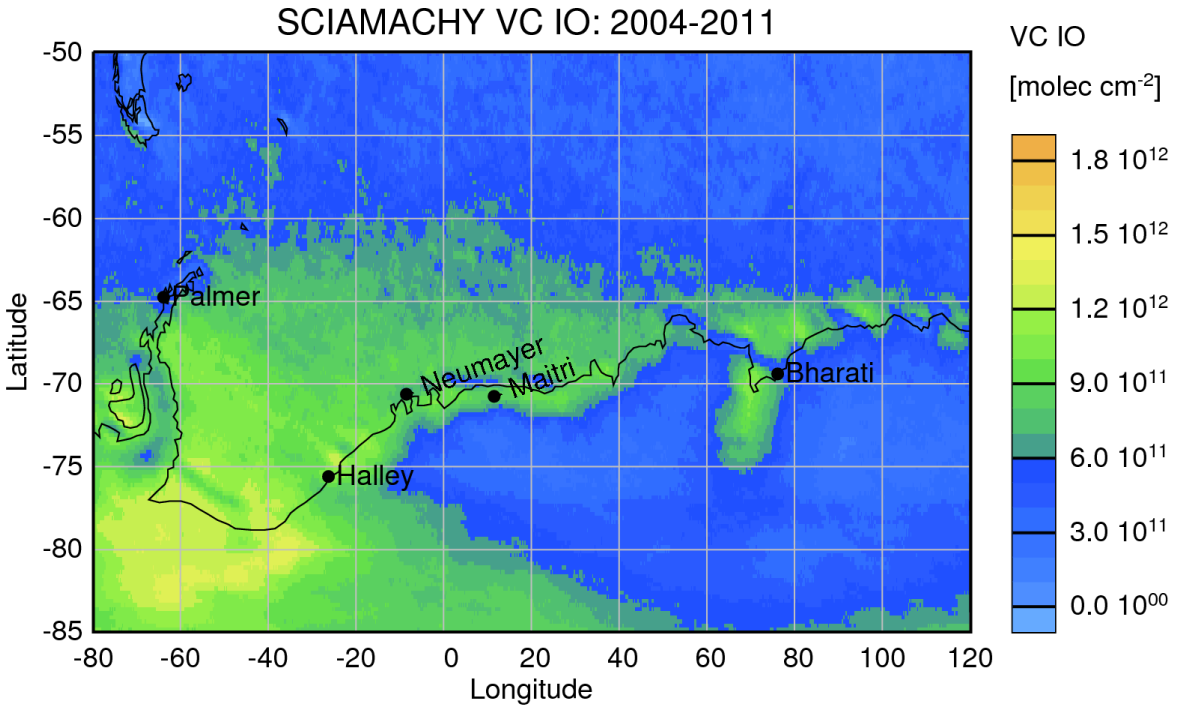

718

719 **Figure 9:** Averaged VCDs of IO as retrieved by SCIAMACHY between 2004-2011are shown.

720 Observations suggest that lower levels of IO are expected at Bharati and Maitri, as compared to

721 Halley Bay and Neumayer.

722

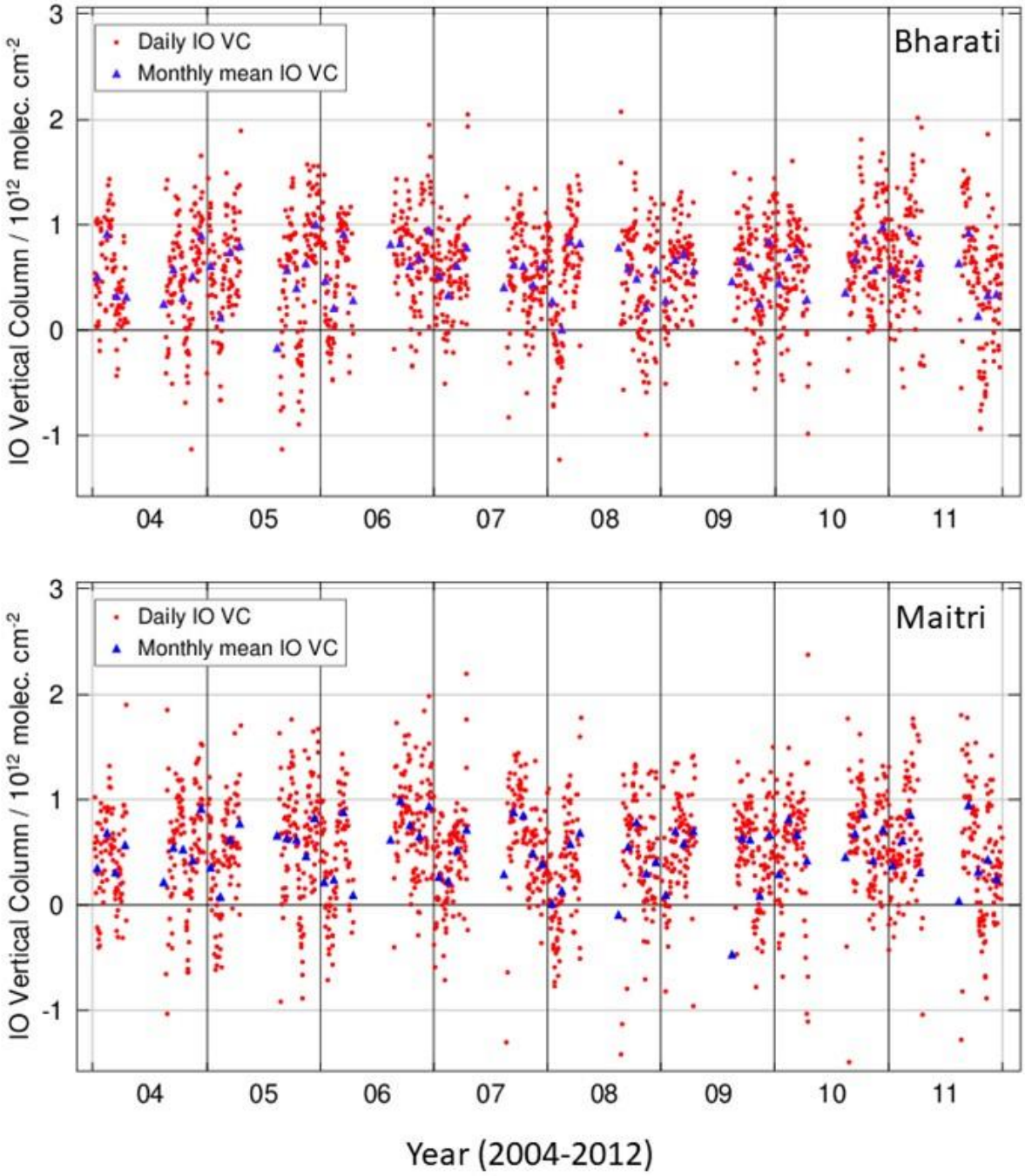

723

724 **Figure 10:** Timeseries of IO VCD observations at the Bharati station as retrieved by
725 SCIAMACHY. The monthly mean values are shown in blue, and the daily datapoints are shown
726 in red.

727